*metals*

MDPI

*Article*

# Mechanism Elucidation of High-Pressure Generation in Cellular Metal at High-Velocity Impact

**Masatoshi Nishi [1], Shigeru Tanaka [2], Akihisa Mori [3], Matej Vesenjak [4], Zoran Ren [4,5] and Kazuyuki Hokamoto [2,*]**

1 Department of Mechanical and Intelligent Systems Engineering, National Institute of Technology (KOSEN), Kumamoto College, Kumamoto 866-8501, Japan; nishima@kumamoto-nct.ac.jp
2 Institute of Industrial Nanomaterials, Kumamoto University, Kumamoto 860-8555, Japan; tanaka@mech.kumamoto-u.ac.jp
3 Department of Mechanical Engineering, Sojo University, Kumamoto 860-0082, Japan; makihisa@mec.sojo-u.ac.jp
4 Faculty of Mechanical Engineering, University of Maribor, 2000 Maribor, Slovenia; matej.vesenjak@um.si (M.V.); zoran.ren@um.si (Z.R.)
5 International Research Organization for Advanced Science and Technology, Kumamoto 860-8555, Japan
* Correspondence: hokamoto@mech.kumamoto-u.ac.jp; Tel.: +81-96-342-3740

**Abstract:** Cellular metals exhibit diverse properties, depending on their geometries and base materials. This study investigated the mechanism of high-pressure generation during the high-velocity impact of unidirectional cellular (UniPore) materials. Cubic UniPore copper samples were mounted on a projectile and subjected to impact loading using a powder gun to induce direct impact of samples. The specimens exhibited a unique phenomenon of high-pressure generation near the pores during compression. We elucidate the mechanism of the high-pressure phenomenon and discuss the pore geometries that contribute to the generation of high pressures.

**Keywords:** cellular metal; high-pressure; high-velocity impact; computational simulation; metal jet



**Citation:** Nishi, M.; Tanaka, S.; Mori, A.; Vesenjak, M.; Ren, Z.; Hokamoto, K. Mechanism Elucidation of High-Pressure Generation in Cellular Metal at High-Velocity Impact. *Metals* **2022**, *12*, 128. https://doi.org/10.3390/met12010128

Academic Editor: Ezio Cadoni

Received: 17 December 2021
Accepted: 6 January 2022
Published: 9 January 2022



## 1. Introduction

Cellular metals are characterised by high porosity that significantly influences their mechanical properties. They can be used in a wide range of fields [1–3] because of their various functions, which depend on the cellular morphology, topology and base material. In cellular materials, research has been conducted to clarify the relationship between the structure, mechanical properties [4–8], and thermal conductivity [9–11], as well as to explore their applications in aerospace [12,13] and medical fields [14–16]. Additionally, the research scope in this field is extensive, including studies on nano-cellular metals [17,18] with cell sizes scaled down to nanometre dimensions.

Although the behaviour of cellular materials under high-velocity impact has already been investigated, only a few studies focus on the high-pressure generation within cellular materials during impact [19–21]. The high-pressure phenomenon has been used in various fields, such as diamond production [22], nanocomposite material preparation, and powder solidification. It has also been applied to synthesise hydrogen-storage materials [23]. Therefore, the investigation of high-pressure generation within cellular materials may lead to further development of future predesigned application-oriented cellular materials. The advantages of the high pressure in each pore of the cellular material are that it can be used to synthesise new materials efficiently in a single experiment, and the high pressure inside the pores makes it easy to recover the synthesised materials.

In this study, the cellular material was accelerated using a powder gun and impacted on a fixed anvil. The testing was captured by a high-speed video camera that confirmed high-pressure generation in the compression process, which was also observed by numerical analysis simulating the impact experiment [20]. This phenomenon is similar to the

study of void collapses on hollow cylinders; however, the mechanism of high pressure generated in cellular materials has not been clarified yet [24]. Therefore, the main objective of this research is to elucidate the generation mechanism of ultra-high pressure and propose a cellular material geometry that can generate even higher pressures by applying the observed mechanism and the metal jet generated during explosive welding.

## 2. Mechanism of High-Pressure Generation

### *2.1. Previous Research Results and Analytical Model*

The samples, test and analysis conditions, and material parameters were the same as those used in the previous study [20]. The projectile, consisting of a copper-based unidirectional porous (UniPore) cube sample [6,7], metal disk, and sabot, was accelerated by a powder gun to 400 m/s and impacted on a fixed anvil. A cubic sample of 17.3 mm on each side was cut from a copper UniPore structure. The porosity of this sample was 0.26, and the average diameter of the pores was in the range of 1.5–1.6 mm. The barrel and impact chamber of the gun were in a near-vacuum state to minimise the air resistance. Details of the experimental methods are described in Chapter 2 of [20].

The computational analysis was performed using the ANSYS AUTODYN version 2021R1 code with a three-dimensional model. In this model, all the materials, i.e., steel, copper and Ultra High Molecular Weight Polyethylene (UHMWPE) are described as a Lagrangian mesh. Based on this model, the complete deformation mechanism and the induced impact force (pressure) during a high-speed collision were analyzed. The equation of state, constitutive equation and material parameters are given in [20]. It is noted here that the effectiveness of this computational model was demonstrated by comparing the experimental and simulation results of the final deformation state after impact, pressure history on the anvil, etc [20].

Figure 1a shows a magnified view of the compression process of the UniPore copper structure. After the sample impacted the anvil, the circular pores first deformed into an arc shape, followed by pore volume decrease, and finally, pore collapse. High pressure was generated when the pore surfaces collided. The highest pressure estimated by computational simulations was approximately 25 GPa, where the red region in Figure 1b was at 2.3 μs. The arc shape of the collapsed pores was also confirmed by observing the cross-sections of the impacted samples [20].

### *2.2. Mechanism of Ultra-High Pressure Generation*

In this section, the mechanism of high-pressure generation around the pores is investigated by computational simulation. Figure 2 shows the position of the pressure gauges positioned around the selected circular pore, at the front of the sample computational model. Gauges 1 and 3 are located on the pore's front and back surfaces, respectively, on the pore's horizontal axis, considering the impact anvil. Gauges 2 and 4 are located above and below the pore, respectively, converging at the arc shape, as shown in Figure 1. Figure 3a shows the velocity vectors at 0.5, 1.0 and 1.5 μs, and Figure 3b shows the velocity vectors at 2.0, 2.1 and 2.2 μs. In Figure 3a, the velocity vectors of the material around the pore on the anvil side are reversed. Figure 3b shows that the velocity vector is towards the centre of the pore. The reason for this gauge arrangement is that the velocities with the x-axis of gauges 1 and 3, and the y-axis of gauges 2 and 4, contribute to the generated pressure at the time of impact.

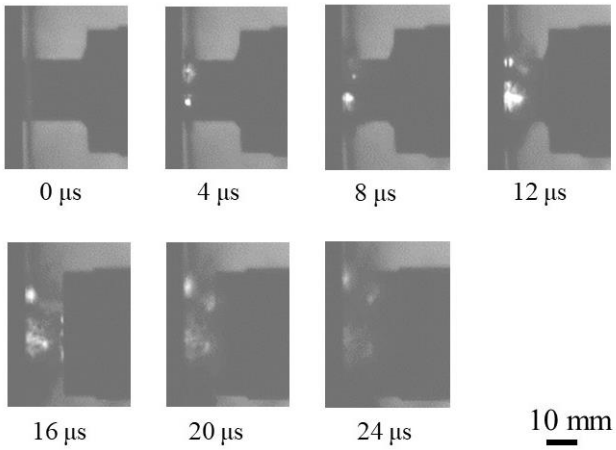


(**a**)

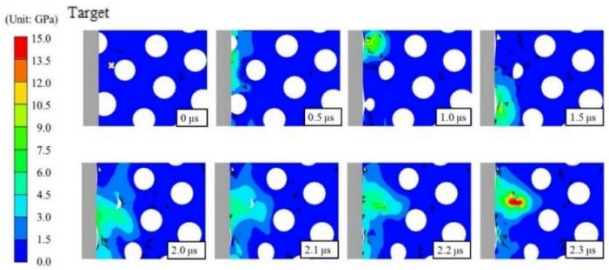


(**b**)

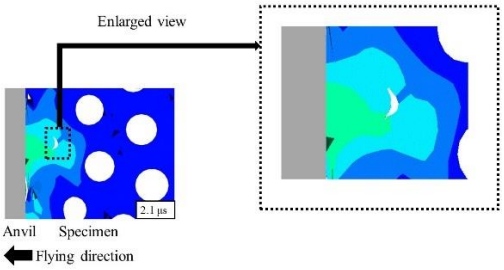


(**c**)

**Figure 1.** Deformation process during impact of copper-based unidirectional porous (UniPore) cube sample: (**a**) observed by the high-speed camera, (**b**) computational simulations, showing local pressure distribution and (**c**) a zoomed, detailed view of the selected arc-shape deformed pore shown in (**b**) at 2.1 μs. Reprinted from [20] with permission from Elsevier.

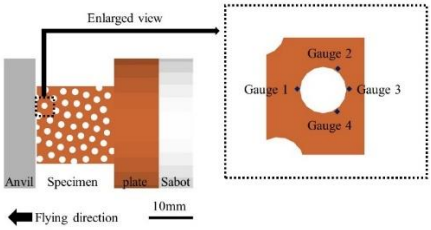


**Figure 2.** Schematic diagram of the computational analysis and gauge positions in the specimen.

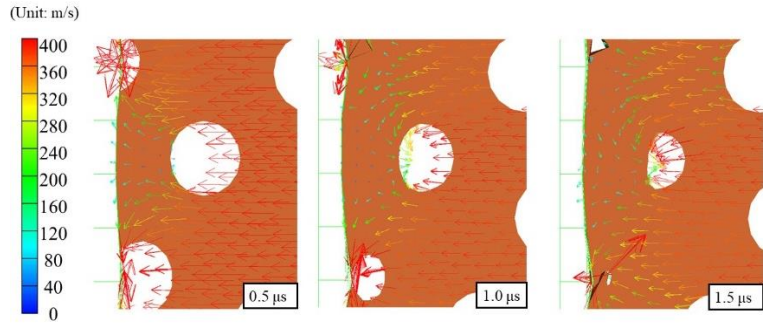


(**a**)

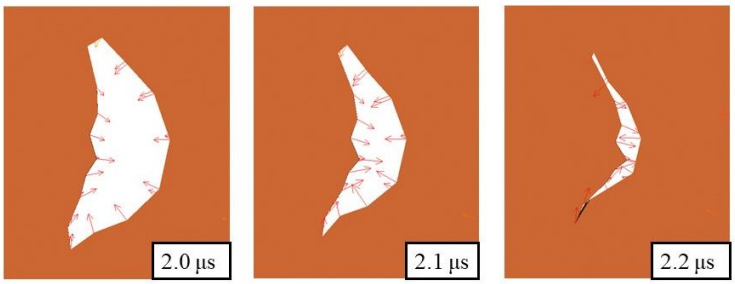


(**b**)

**Figure 3.** Absolute velocity vectors; (**a**) shows local distribution (**b**) shows only the pore to make it easier to see the vectors.

Figure 3a shows that the high pressure caused by the collapse of the neighbouring pore has little effect on the target pore, because there is a certain distance between target pore and the neighbouring pore in this model. However, when the pores are close to each other, this effect needs to be considered.

The positive longitudinal direction (right) of the computational model and the flying direction of the sample (left) were opposite. According to Figure 4, the velocity of the pore's front surface (gauge 1) reduced fast to zero when the specimen collided with the anvil, and then increased in the reverse direction to finally surpass 400 m/s, just before colliding with the opposite surface at the back of the pore. The velocity of the pore's back surface (gauge 3) remained at approximately −400 m/s until the pore surface collision and inevitable collapse. The combined impact velocity of the pore surface at collapse was estimated at 800 m/s. The pressure peak generated during the copper pore surface collisions can be calculated using an impedance matching technique that uses the Rankine–Hugoniot equation relating pressure to particle velocity [25]. Figure 5 shows the impedance matching relationship for a copper-to-copper collision with an initial velocity of 800 m/s, leading to a pressure intersection of about 16 GPa. The pressure intersection in Figure 5, that is, the

potentially generated pressure value, is calculated as 16 GPa. Since the pressure estimated by the velocity in the x-axis alone does not reach the 25 GPa estimated by the computational analysis [20], the next step is to investigate the transversal direction.

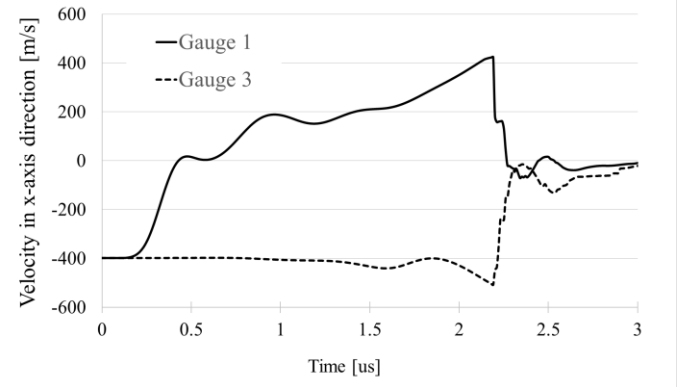


**Figure 4.** Velocity histories at gauges 1 and 3 in x−axis estimated by computational simulation.

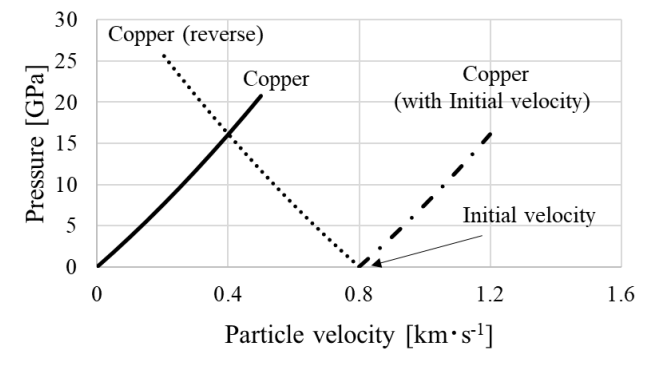


**Figure 5.** Impedance matching relationship for a copper−to−copper collision with initial velocity 800 m/s in x−axis.

The velocities of the pore surface at gauges 2 and 4 in the transversal direction were observed next (Figure 6). The positive transversal direction of the computational model in Figure 2 is oriented upwards. The top of the pore (gauge 2) shows a gradual transversal velocity increase towards the pore centre (downward movement) due to arc-shape deformation, reaching approximately −200 m/s at total pore collapse. The bottom of the pore (gauge 4) also moves towards the pore centre with a positive increasing transversal velocity following the same deformation mechanism, reaching approximately 480 m/s at pore collapse. The velocity difference is due to varying local structure stiffness around the observed pore as a consequence of the different positioning of the neighboring pores. Assuming collision only in the y-axis direction, the generated pressure value was calculated by the impedance matching method to be 11.8 GPa.

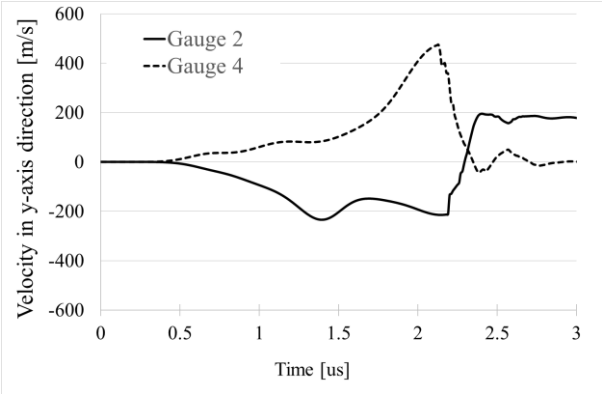


**Figure 6.** Velocity histories at gauges 2 and 4 in y−axis estimated by computational simulation.

Figures 4 and 6 show that the pores were closed by the convergence of high velocities in the x- and y-axes; that is, a high pressure is generated by the convergence of velocity in these two axes.

The observed velocities along the second transversal orientation aligned with the pore are very small compared to the velocities observed in the other two directions, and its effects on the generated pressure are consequently negligible.

## 3. Differences in Pressure Depending on Geometry of the Specimen

In Section 2, we explained the mechanism of high-pressure generation related to our previous studies. In this section, we apply the same mechanism to propose a cellular material geometry, shown in Figure 7, that can obtain even higher pressures than presented in Section 2. The analysis conditions and material parameters were the same as those in previous studies [20].

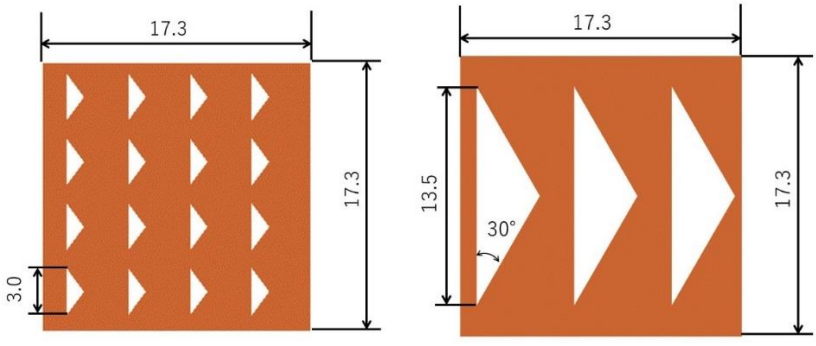


**Figure 7.** The shape of the proposed cubic cellular samples. (**a**) Sample 1, pore dimensions: Isosceles triangle with a base of 3 mm and a height of 1.5 mm (**b**) Sample 2.

The circular pore shape of the sample in Section 2 was changed to a triangular shape, which is estimated to produce a higher pressure due to the convergence of the material at a single point when the pore is completely closed. The shape of the proposed cubic cellular samples are shown in Figure 7. Sample 2 is a model for copper-to-copper collisions, where the metal jet is generated at an angle of 20–30° from the welding window, as studied in explosion welding [26]. Here, metal jets are generated in the compression process and collide to achieve a high pressure.

### *3.1. Proposed Cellular Material Shape (Sample 1)*

An enlarged view of the compression process of sample 1 is shown in Figure 8, and the pressure history of the most stressed discretisation point around the pore is shown

in Figure 9. The material around the pore gathers at one point when the pore is completely closed. Therefore, a large pressure of approximately 70 GPa can be expected by Figures 8 and 9. Although the impedance matching method cannot be applied to this proposed example because it is a triple-point collision, the collision velocity of about 1000 m/s is obtained at point x in Figure 8. Therefore, we can expect to obtain a high pressure as shown in Figure 9.

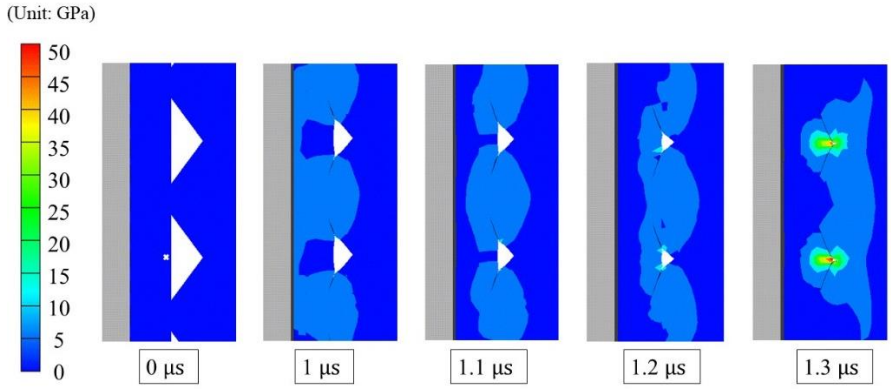


**Figure 8.** Local pressure distribution and pore deformation marked by "x" (the cross-sectional front view. The anvil, plate and sabot are not displayed).

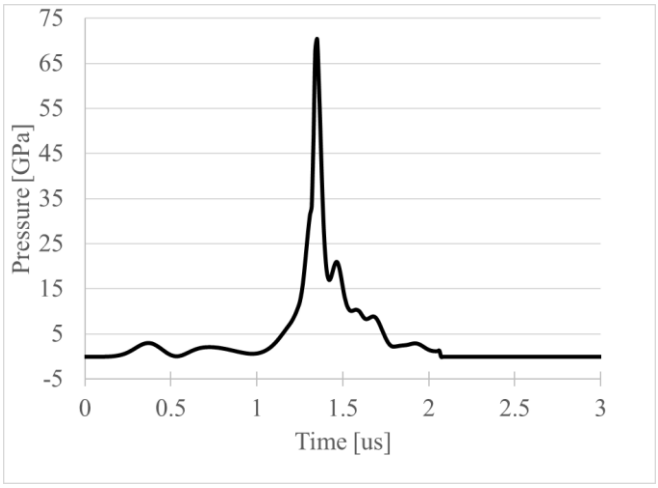


**Figure 9.** Local pressure history at "x" marked in Figure 8 estimated by computational simulation.

### *3.2. Proposed Cellular Material Shape (Sample 2)*

Figure 10a shows the schematic diagram used for explosive welding, where point A moves toward point B with a velocity $V_p$, and point O moves toward point B with a velocity of $V_w$, creating a metal jet between edges OA and OB depending on the conditions. The relationship between the velocity and angle is expressed by the following equation, where β is the collision angle, and $V_w$ is the welding velocity [26,27].

$$\frac{1}{2}V_p = V_d \sin\frac{\beta}{2} \quad (1)$$

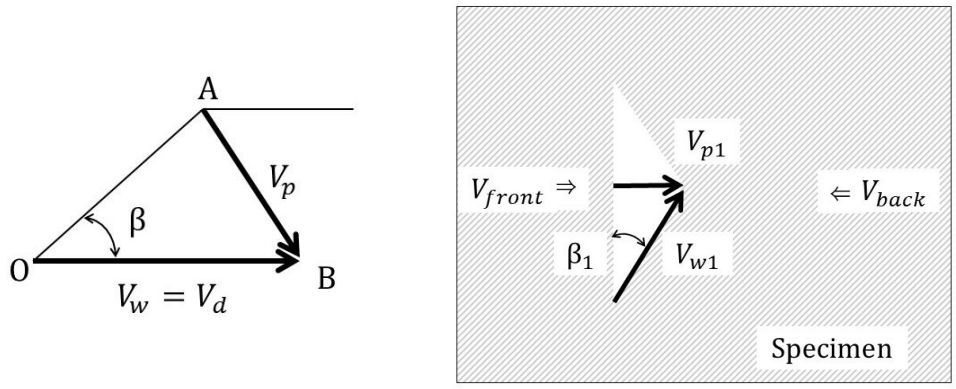


**Figure 10.** Geometrical analysis (**a**) Typical explosive welding, (**b**) proposed structure (sample 2).

Figure 10b shows a schematic diagram of the proposed structure corresponding to Figure 10a, where $V_{p1} = abs(V_{front}) + abs(V_{back})$, subscript 1 corresponds to Figure 10b, and $V_{front}$ and $V_{back}$ are the velocity vectors of the base material around the pore.

The pressure is expected to be higher due to the convergence effect at a single point at the time of complete closure when angle β is large. Here, the inclination angle β was set to 30°.

The computationally estimated compression process of the proposed cellular material with triangular pore geometry is illustrated in Figure 11. The pore gradually compressed from both transversal triangle corners towards the apex on the sabot side, and consequently converged to a single point at the time of complete pore collapse. After the first pore collapsed, a pressure wave was generated towards the next pore, indicating that the phenomenon of high-pressure generation continued. Figure 12 shows pressure history near pore estimated by computational simulation and the enlarged view of compression process Figure 11 at 5.1 µs Although this computational simulation can not reproduce the formation of the metal jet, it is expected that even higher pressures will be generated in the experiment due to increased pore collapse followed by the metal jet appearance.

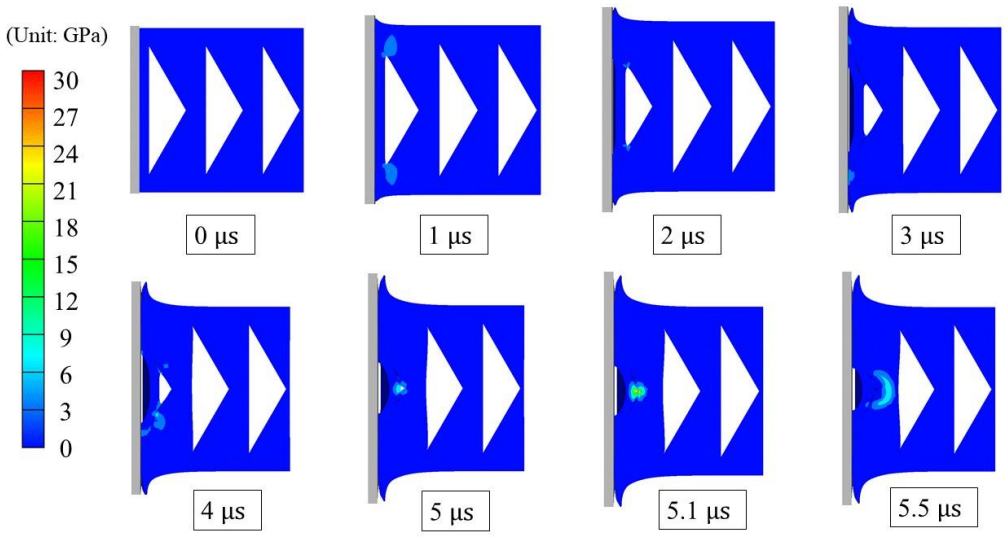


**Figure 11.** Compression process with pressure contour (the cross-sectional front view. The anvil, plate and sabot are not displayed).

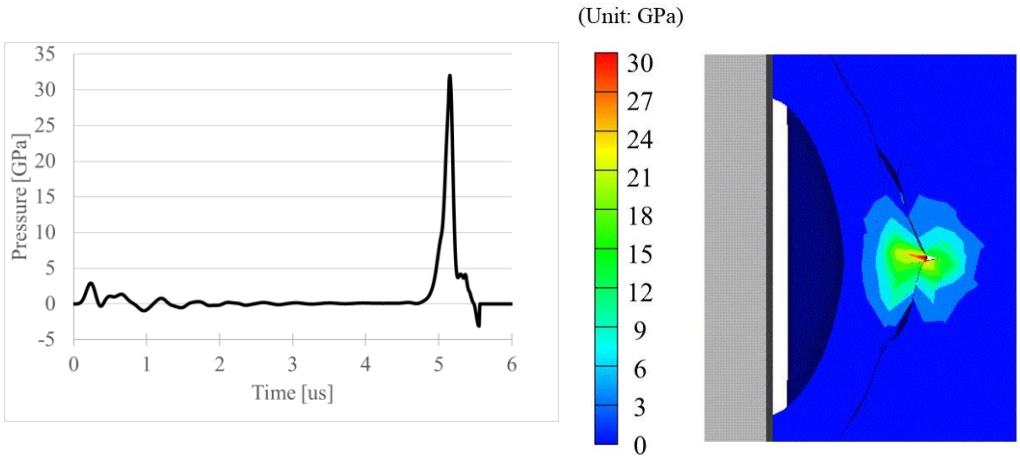


(**a**) (**b**)

**Figure 12.** Computational simulation results; (**a**) Pressure history near pore (**b**) enlarged view at 5.1 μs.

### *3.3. Advantages of High-Pressure Generation with Cellular Materials*

The observed high pressures produced in impact deformation of the UniPore cellular material can be used for diamond synthesis, by placing carbon on the inside surface of the pores. Althougth it is necessary to pay attention to the effect of the pressure generated in the neighboring pores when the pores are close to each other in a porous geometry, this method has the following advantages:

- The advantages of the high pressure in each pore of the cellular material are that it can be used to synthesise new materials efficiently in a single experiment.
- The number and shape of the pores can be easily changed, and the sample preparation is relatively simple using a wire electrical discharge machine.
- High pressure is generated inside the cellular material, so the newly synthesised material is easy to recover.
- Colliding the metal jets of the base material is expected to contribute to new material fabrication. Furthermore, it can be applied to the convergence of metal jets using a conical concave metal block [28].
- The adiabatic compression of air can be achieved by filling the pores with air capsules.

## 4. Conclusions

In this study, we investigated the mechanism of high-pressure generation using unidirectional cellular (UniPore) materials. The study focused on the velocity of the base material around the pore during the high-velocity compression forming process, using a powder gun to induce direct impact of samples. The circular pores deformed in an arc-like shape during impact, leading to a high-speed collision of opposite pore surfaces at pore collapse in the longitudinal direction of the impact. A cellular material with a triangular pore shape can produce even higher pressures by applying metal jets, as observed in explosive welding studies.

**Author Contributions:** Conceptualisation, K.H.; methodology, K.H.; validation, M.N., S.T. and A.M.; investigation, M.N., S.T., A.M. and M.V.; Resources, S.T.; Data evaluation, M.N. and S.T.; writing-original draft preparation, M.N.; writing—review and editing, M.V., Z.R. and K.H.; supervision, Z.R. and K.H.; project administration, Z.R. and K.H. All authors have read and agreed to the published version of the manuscript.

**Funding:** The authors acknowledge the financial supports by the AMADA Foundation (AF-2019005-A3) and the Slovenian Research Agency (research core funding No. P2-0063).

**Data Availability Statement:** Not applicable.

**Conflicts of Interest:** There are no conflict of interest.

## References


1. Ashby, M.; Evans, A.; Fleck, N.; Gibson, L.; Hutchinson, J.; Wadley, H.; Delale, F. Metal Foams: A Design Guide. *Appl. Mech. Rev.* **2001**, *54*, B105–B106. [CrossRef]
2. Shapovalov, V. Porous Metals. *MRS Bull.* **1994**, *19*, 24–28. [CrossRef]
3. Banhart, J. Manufacture, Characterisation and Application of Cellular Metals and Metal Foams. *Prog. Mater. Sci.* **2001**, *46*, 559–632. [CrossRef]
4. Vesenjak, M.; Duarte, I.; Baumeister, J.; Göhler, H.; Krstulović-Opara, L.; Ren, Z. Bending Performance Evaluation of Aluminium Alloy Tubes Filled with Different Cellular Metal Cores. *Compos. Struct.* **2020**, *234*, 111748. [CrossRef]
5. Peixinho, N.; Carvalho, O.; Areias, C.; Pinto, P.; Silva, F. Compressive Properties and Energy Absorption of Metal-Polymer Hybrid Cellular Structures. *Mater. Sci. Eng. A* **2020**, *794*, 139921. [CrossRef]
6. Vesenjak, M.; Hokamoto, K.; Sakamoto, M.; Nishi, T.; Krstulović-Opara, L.; Ren, Z. Mechanical and Microstructural Analysis of Unidirectional Porous (UniPore) Copper. *Mater. Des.* **2016**, *90*, 867–880. [CrossRef]
7. Hokamoto, K.; Vesenjak, M.; Ren, Z. Fabrication of Cylindrical Uni-Directional Porous Metal with Explosive Compaction. *Mater. Lett.* **2014**, *137*, 323–327. [CrossRef]
8. Zuo, Q.; He, K.; Mao, H.; Dang, X.; Du, R. Manufacturing Process and Mechanical Properties of a Novel Periodic Cellular Metal with Closed Cubic Structure. *Mater. Des.* **2018**, *153*, 242–258. [CrossRef]
9. Bai, X.; Nakayama, A. Quick Estimate of Effective Thermal Conductivity for Fluid-Saturated Metal Frame and Prismatic Cellular Structures. *Appl. Therm. Eng.* **2019**, *160*, 114011. [CrossRef]
10. Sato, Y.; Yuki, K.; Abe, Y.; Kibushi, R.; Unno, N.; Hokamoto, K.; Tanaka, S.; Tomimura, T. Heat Transfer Characteristics of a Gas Flow in Uni-Directional Porous Copper Pipes. In Proceedings of the International Heat Transfer Conference, Beijing, China, 10–15 August 2018.
11. Fiedler, T.; Borovinšek, M.; Hokamoto, K.; Vesenjak, M. High-Performance Thermal Capacitors Made by Explosion Forming. *Int. J. Heat Mass Transf.* **2015**, *83*, 366–371. [CrossRef]
12. Parsons, E.M. Lightweight Cellular Metal Composites with Zero and Tunable Thermal Expansion Enabled by Ultrasonic Additive Manufacturing: Modeling, Manufacturing, and Testing. *Compos. Struct.* **2019**, *223*, 110656. [CrossRef]
13. Hohe, J.; Hardenacke, V.; Fascio, V.; Girard, Y.; Baumeister, J.; Stöbener, K.; Weise, J.; Lehmhus, D.; Pattofatto, S.; Zeng, H.; et al. Numerical and Experimental Design of Graded Cellular Sandwich Cores for Multi-Functional Aerospace Applications. *Mater. Des.* **2012**, *39*, 20–32. [CrossRef]
14. Prabhu, A.; Gadgil, M. Trace Metals in Cellular Metabolism and Their Impact on Recombinant Protein Production. *Process Biochem.* **2021**, *110*, 251–262. [CrossRef]
15. Jaivignesh, M.; Babu, A.S.; Arumaikkannu, G. In-Vitro Analysis of Titanium Cellular Structures Fabricated by Direct Metal Laser Sintering. *Mater. Today Proc.* **2020**, *22*, 2372–2377. [CrossRef]
16. Attar, H.; Ehtemam-Haghighi, S.; Soro, N.; Kent, D.; Dargusch, M.S. Additive Manufacturing of Low-Cost Porous Titanium-Based Composites for Biomedical Applications: Advantages, Challenges and Opinion for Future Development. *J. Alloys Compd.* **2020**, *827*, 154263. [CrossRef]
17. Wu, Q.; Luo, M.; Han, J.; Peng, W.; Zhao, Y.; Chen, D.; Peng, M.; Liu, J.; de Groot, F.M.F.; Tan, Y. Identifying Electrocatalytic Sites of the Nanoporous Copper–Ruthenium Alloy for Hydrogen Evolution Reaction in Alkaline Electrolyte. *ACS Energy Lett.* **2020**, *5*, 192–199. [CrossRef]
18. Qin, C.; Zheng, D.; Hu, Q.; Zhang, X.; Wang, Z.; Li, Y.; Zhu, J.; Ou, J.Z.; Yang, C.; Wang, Y. Flexible Integrated Metallic Glass-Based Sandwich Electrodes for High-Performance Wearable All-Solid-State Supercapacitors. *Appl. Mater. Today* **2020**, *19*, 100539. [CrossRef]
19. Novak, N.; Hokamoto, K.; Vesenjak, M.; Ren, Z. Mechanical Behaviour of Auxetic Cellular Structures Built from Inverted Tetrapods at High Strain Rates. *Int. J. Impact Eng.* **2018**, *122*, 83–90. [CrossRef]
20. Nishi, M.; Tanaka, S.; Vesenjak, M.; Ren, Z.; Hokamoto, K. Experimental and Computational Analysis of the Uni-Directional Porous (UniPore) Copper Mechanical Response at High-Velocity Impact. *Int. J. Impact Eng.* **2020**, *136*, 103409. [CrossRef]
21. Tanaka, S.; Hokamoto, K.; Irie, S.; Okano, T.; Ren, Z.; Vesenjak, M.; Itoh, S. High-Velocity Impact Experiment of Aluminum Foam Sample Using Powder Gun. *Measurement* **2011**, *44*, 2185–2189. [CrossRef]
22. Tetsuo, I.; Ayako, K.; Shizue, S.; Toru, I.; Hitoshi, S. Ultrahard Polycrystalline Diamond from Graphite. *Nature* **2003**, *421*, 599–600.
23. Kamegawa, A.; Kataoka, R.; Okadaa, M. High Pressure Synthesis of Novel Li-TM Hydrides (TM = Nb, Ta). *Energy Procedia* **2012**, *29*, 276–282. [CrossRef]
24. Nemat-Nasser, S.; Okinaka, T.; Nesterenko, V. Experimental Observation and Computational Simulation of Dynamic Void Collapse in Single Crystal Cooper. *Mater. Sci. Eng. A* **1998**, *249*, 22–29. [CrossRef]
25. Meyers, M.; Murr, E.L. *Shock Waves and High-Strain-Rate Phenomena in Metals*; Springer: London, UK, 1981.
26. Crossland, B. *Explosive Welding of Metals and Its Application*; Clarendon Press: Oxford, UK, 1982.

27. Grignon, F.; Benson, D.; Vecchio, K.S.; Meyers, M.A. Explosive Welding of Aluminum to Aluminum: Analysis, Computations and Experiments. *Int. J. Impact Eng.* **2004**, *30*, 1333–1351. [CrossRef]
28. Kira, A.; Takaenoki, D.; Hamashima, H.; Tomoshige, R.; Fujita, M.; Hokamoto, K.; Itoh, S. Optical Observation of Extremely High Impulsive Pressure Generator Using Collision of High Velocity Metal Jets. *Mater. Sci. Forum* **2004**, *465*, 265–270. [CrossRef]